Unusual two-dimensional behavior of iron-based superconductors with low anisotropy

A. A. Kalenyuk,[1,2] A. Pagliero,[1] E. A. Borodianskyi,[1] S. Aswartham,[3] S. Wurmehl,[3,4] B. Büchner,[3,4]
D. A. Chareev,[5,6,7] A. A. Kordyuk,[2,8] and V. M. Krasnov[1,*]

[1]*Department of Physics, Stockholm University, AlbaNova University Center, SE-10691 Stockholm, Sweden*
[2]*Institute of Metal Physics of National Academy of Sciences of Ukraine, 03142 Kyiv, Ukraine*
[3]*Leibniz Institute for Solid State and Materials Research Dresden IFW, Institute for Solid State Research, 01069 Dresden, Germany*
[4]*Institute for Solid State Physics, TU Dresden, 01062 Dresden, Germany*
[5]*Institute of Experimental Mineralogy, Russian Academy of Sciences, 142432 Chernogolovka, Russia*
[6]*Institute of Physics and Technology, Ural Federal University, 620002 Ekaterinburg, Russia*
[7]*Institute of Geology and Petroleum Technologies, Kazan Federal University, 420008 Kazan, Russia*
[8]*Kyiv Academic University, 03142 Kyiv, Ukraine*

We study angular-dependent magnetoresistance in iron-based superconductors $Ba_{1-x}Na_xFe_2As_2$ and $FeTe_{1-x}Se_x$. Both superconductors have relatively small anisotropies $\gamma \sim 2$ and exhibit a three-dimensional (3D) behavior at low temperatures. However, we observe that they start to exhibit a profound two-dimensional behavior at elevated temperatures and in applied magnetic field parallel to the surface. We conclude that the unexpected two-dimensional (2D) behavior of the studied low-anisotropic superconductors is not related to layeredness of the materials, but is caused by appearance of surface superconductivity when magnetic field exceeds the upper critical field $H_{c2}(T)$ for destruction of bulk superconductivity. We argue that the corresponding 3D-2D bulk-to-surface dimensional transition can be used for accurate determination of the upper critical field.

I. INTRODUCTION

The importance of low dimensionality for achieving high-temperature superconductivity is a long-standing question [1]. Cuprate superconductors do have a quasi-two-dimensional layered structure, confirmed by observation of the intrinsic Josephson effect [2–4]. But, iron-based superconductors, which contain both three-dimensional (3D) and two-dimensional (2D) electronic bands [5,6], may either be highly anisotropic [7,8], moderately anisotropic [9,10], or nearly isotropic [11]. Therefore, the role of dimensionality for iron-based superconductors remains to be understood.

The well-known signature of layeredness is a dimensional 3D-2D crossover. It occurs upon decreasing of temperature and is due to temperature variation of the coherence length $\xi(T)$ [12–17]. Close to T_c, the $\xi(T)$ is larger than the separation between layers s and the superconductor is in a spatially averaged 3D state. The 3D-2D transition takes place upon decreasing T when the out-of-plane coherence length $\xi_\perp(T_{2D})$ becomes smaller than $s/\sqrt{2}$ [13,14]. The decoupling and subsequent 3D-2D crossover may also take place at a fixed T upon increasing of magnetic field, which suppresses superconductivity in intermediate weakly superconducting layers [16]. A related dimensional transition occurs in the vortex structure from 3D Abrikosov vortex lines to 2D pancake vortices [18]. For the dimensional crossover to take place, the anisotropy γ has to be larger than the critical value $\gamma_{cr} \simeq \sqrt{2}\xi_\parallel(0)/s$, where $\xi_\parallel = \gamma\xi_\perp$ is the in-plane coherence length. For high-temperature superconductors $\xi_\parallel(0) \sim 3$–5 nm, $s \lesssim 1$ nm and the critical anisotropy $\gamma_{cr} \sim 4$–10. This condition is not satisfied at least for some iron pnictides [11]. This raises a question if superconductivity ever behaves as 2D

in iron-based superconductors as in cuprates. The most clear evidences for layeredness, such as the observation of interlayer Josephson effect [15] and intrinsic pinning [16], have not been found yet for iron-based compounds. On the other hand, a cusplike 2D behavior of angular dependence of magnetoresistance observed for some iron-based superconductors [19,20] reminds the aforementioned 3D-2D crossover in layered superconductors [12,17].

Recently, it has been demonstrated that 2D superconductivity may be observed even in isotropic superconductors, such as Nb [21] at sufficiently high magnetic fields. This is caused by appearance of 2D surface superconductivity. Surface superconductivity (SSC) [22] exists in a thin surface layer with the thickness of the order of ξ at fields $H_{c2} < H < H_{c3}$ above the upper critical field for destruction of bulk superconductivity H_{c2}, but below the third critical field H_{c3}. For conventional superconductors $H_{c3}/H_{c2} \simeq 1.7$, but this ratio depends on parameters of the superconductor such as cleanliness [22] and the quality of the surface [22–24]. Because SSC is sensitive to the surface conditions, it has long been considered as a fragile phenomenon that exists only in clean and well-polished samples. However, recently it has been demonstrated that the SSC is very robust and exists even in polycrystalline films and in perpendicular magnetic fields [21]. Indeed, SSC has been observed in a variety of superconductors, including conventional low-T_c [21,24–26], MgB_2 [27,28], and some iron pnictides [29].

In this work we study angular dependence of magnetoresistance in $Ba_{1-x}Na_xFe_2As_2$ and $FeTe_{1-x}Se_x$ single crystals. Superconductivity in both compounds is of a slightly anisotropic 3D character. However, we observe that in applied magnetic field they start to exhibit a profound 2D behavior with increasing temperature. We demonstrate that the 2D cusplike angular dependence of magnetoresistance occurs in the whole region of a smeared superconducting transition.

*Vladimir.Krasnov@fysik.su.se

Contrary to the conventional 3D-2D crossover in layered superconductors, the observed 3D-2D transition is temperature inverted because it occurs upon *increasing* (rather than decreasing) of temperature. We discuss possible origins of the unexpected 2D behavior in low-anisotropic iron-based superconductors and conclude that it is caused by persistence of surface superconductivity at magnetic field above the bulk H_{c2}. We argue that the corresponding bulk (3D) to surface (2D) dimensional transition can be used for accurate determination of H_{c2} even in case of a broad and smeared superconducting transition.

II. EXPERIMENT

We study magnetoresistance of two types of iron-pnictide $Ba_{1-x}Na_xFe_2As_2$ and iron-chalcogenide $Fe_{1+\delta}Te_{1-x}Se_x$ superconductors. The pnictide crystals were grown using a self-flux high-temperature solution growth technique [30]. The Na substitution, similarly to K substitution in $Ba_{1-x}K_xFe_2As_2$ [10], results in hole doping that leads to the suppression of the spin-density-wave order and induces superconductivity up to 34 K for $x = 0.4$ [31]. Here, we used slightly underdoped $Ba_{1-x}Na_xFe_2As_2$ crystals ($x = 0.35$–0.4) from the same batch, as studied in Ref. [30]. Detailed characterization of those crystals, including specific-heat measurements and angular-resolved photoemission spectroscopy, can be found in Ref. [30]. The quality of crystals was investigated by energy-dispersive x-ray spectroscopy. The composition and the dopant (Na) concentration was obtained by averaging over several parts of each crystal. The standard deviation for the pristine crystals with nominal values $x = 0.35$–0.40 was 0.01. The small standard deviation indicates uniform distribution of Na and a good homogeneity of the crystals.

The $Fe_{1+\delta}Te_{1-x}Se_x$ crystals with $x \simeq 0.28$ were grown in evacuated quartz ampoules using the KCl/NaCl flux technique with a constant temperature gradient (for details see Refs. [32,33]). The $FeSe_xTe_{1-x}$ samples show the superconducting transition temperature that varies from 12 to 15 K with a broad maximum at around $x = 0.3-0.4$. Such crystals exhibit Curie-Weiss behavior at temperatures above 100 K, suggesting the coexistence of superconductivity and magnetic order. However, there are indications of possible phase separation in those compounds [32,34]. The phase separation is indeed confirmed below in the studied crystals.

Figure 1 shows an image (top panel) of one of the studied samples and a 3D sketch (middle panel). Pnictide and chalcogenide samples were fabricated in the manner, similar to cuprate mesa structures [35]. First, a single crystal was glued to a sapphire substrate by an epoxy glue with the *c*-axis oriented perpendicularly to the substrate. The crystal was cleaved along the *ab* planes (easy cleavage plane) and covered by the first metallization layer (Nb). After that, a long narrow line in Nb (a diagonal stripe in Fig. 1) was patterned using photolithography and reactive ion etching. Unlike cuprates, iron-based superconductors form a good metallic contact with various metals. Therefore, in order to avoid short-circuiting outside the contact area, the surface of the crystal around the long Nb line was carefully isolated by a SiO_2 layer and epoxy.
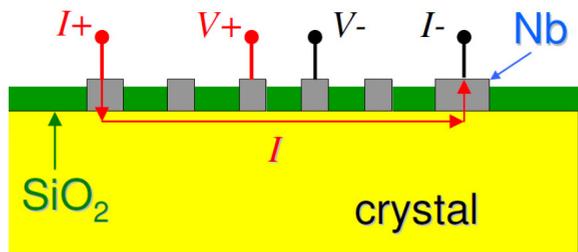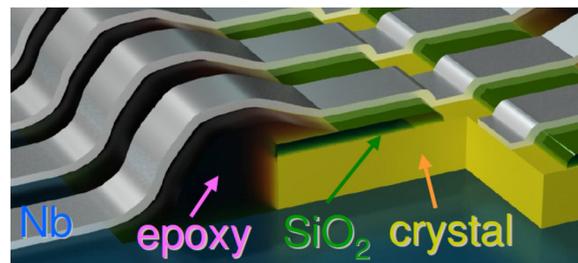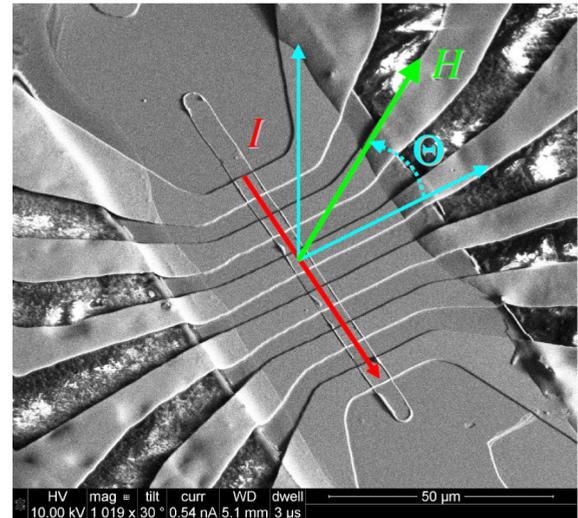
FIG. 1. The top panel shows scanning electron microscope image of one of the studied samples. The middle panel represents a 3D sketch of the sample. The bottom panel shows contact configuration used for four-probe measurement of the in-plane resistance.

After that, a second metallization layer (Nb) is deposited by (dc+rf) magnetron sputtering and six electrodes are patterned across the window in the insulating layer by photolithography. Subsequent reactive ion etching results in six small contacts in a row with attached electrodes at the top. A long (several hours) processing time in deposition and plasma etching chambers is equivalent to soft vacuum annealing. This leads to a reduction of the doping level reflected in a modest reduction of T_c. The exact doping level is not important for the results presented below.

Measurements were performed in a gas-flow ^{4}He cryostat in a temperature range down to 1.8 K and magnetic field H up to 17 T. Samples were mounted on a rotatable sample holder with the alignment accuracy better than $0.02°$. Details of the measurement setup can be found in Ref. [36]. In-plane resistance of our samples is measured in a four-probe configuration: current is sent through the outmost contacts,
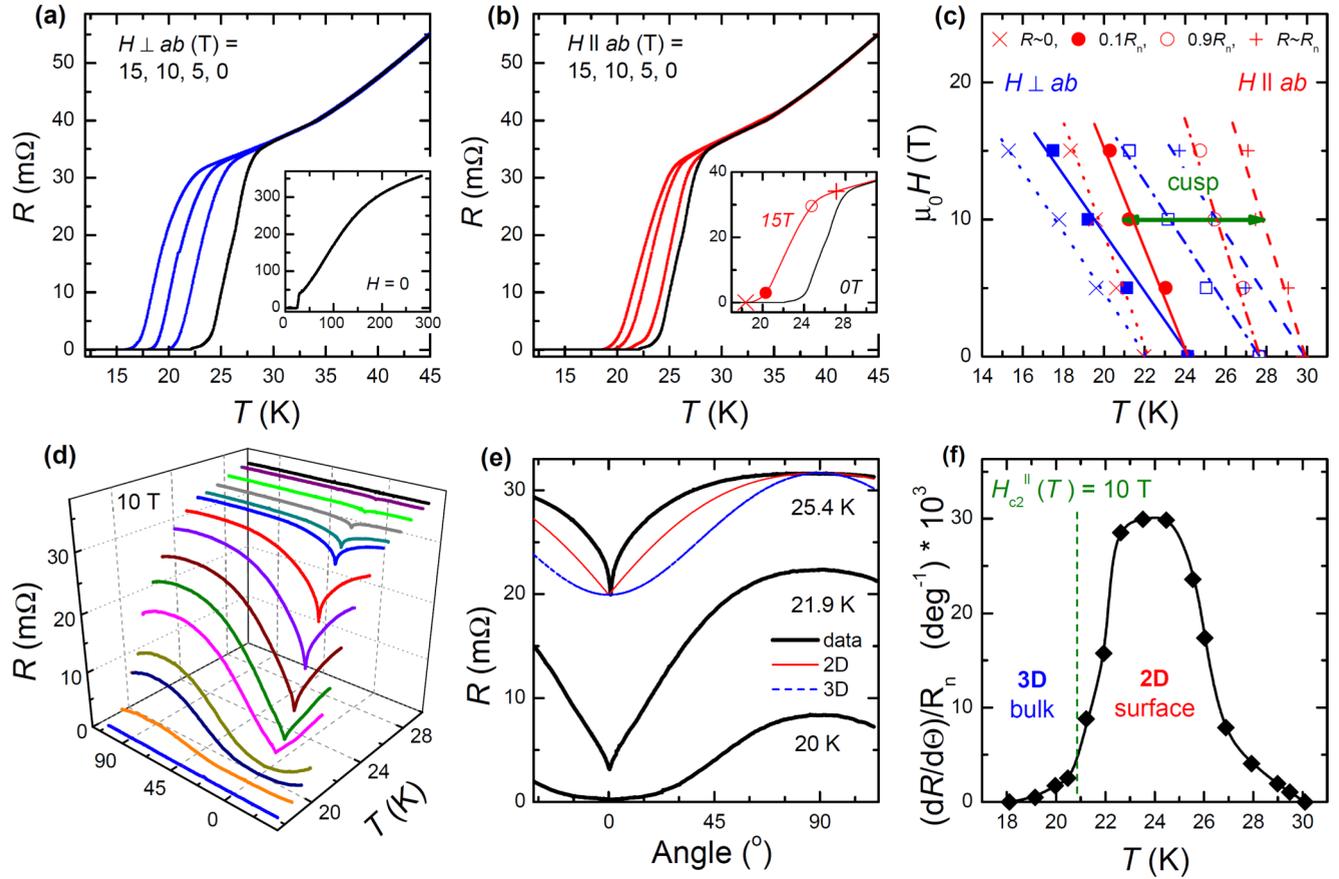
FIG. 2. Experimental characteristics of a slightly underdoped $Ba_{1-x}Na_xFe_2As_2$ single crystal $N.1$. (a), (b) In-plane resistance versus temperature in (a) perpendicular and (b) parallel fields of 0, 5, 10, and 15 T. Inset in (a) shows $R(T)$ at zero field in a broader T range. Inset in (b) shows zoomed-in part of $R(T)$ at $H_\parallel = 0$ and 15 T. Symbols demonstrate determination criteria for 0%, 10%, 90%, and 100% of the resistive transition. (c) Temperature dependencies of the bottom $R \sim 0$ (crosses, dotted lines), 10% (solid symbols and lines), 90% (open symbols, dashed-dotted lines), and the top $R \sim R_n$ (plus symbols, dashed lines) of the resistive transition in perpendicular (blue) and parallel (red) fields. The horizontal arrow indicates the range of temperatures at which the 2D cusp occurs in angular-dependent magnetoresistance at 10 T. (d), (e) Angular dependence of resistance at 10 T and different temperatures. Note appearance of a 2D cusp at elevated temperatures, indicating occurrence of surface superconductivity. Thin red and blue lines in (e) represent standard angular dependencies of flux-flow resistances in 2D and 3D cases, respectively, for a given amplitude $R(90°) - R(0°)$ at $T = 25.4$ K. (f) The sharpness of the cusp versus T for the data from (d). A rapid onset of the cusp at $T > 21$ K manifests the unusual temperature-inverted 3D-2D transition (dashed line).

voltage is measured over the two inner unbiased contacts, as shown in the bottom panel of Fig. 1.

III. RESULTS

A. 2D behavior in $Ba_{1-x}Na_xFe_2As_2$ crystals

Figures 2(a) and 2(b) show the in-plane resistance versus temperature for a slightly underdoped $Ba_{1-x}Na_xFe_2As_2$ crystal $N.1$ measured in magnetic fields of 0, 5, 10, and 15 T perpendicular [Fig. 2(a)] and parallel [Fig. 2(b)] to ab planes. Inset in Fig. 2(a) shows $R(T)$ at $H = 0$ in a broad T range. The crystal has a $T_c \sim 28$ K and a characteristic $R(T)$ shape typical for slightly underdoped $Ba_{1-x}Na_xFe_2As_2$ pnictides with $x \simeq 0.35$ [30]. The resistive transition $R(T)$ in zero field is about 4 K broad and the width is only slightly changing with field.

Figure 2(c) represents field-temperature diagram of resistive transitions in parallel (red) and perpendicular (blue) to ab-plane field orientations. Crosses (dotted lines) and pluses (dashed lines) correspond to bottom and top of the

transitions $R(T) \simeq 0$ and $R(T) \simeq R_n$, solid symbols (solid lines) and open symbols (dashed-dotted lines) correspond to 10% $R(T) \simeq 0.1R_n$ and 90% $R(T) \simeq 0.9R_n$ of the transitions, respectively. Determination of those points is demonstrated by the corresponding symbols in the inset in Fig. 2(b) for $H_\parallel = 15$ T.

In order to investigate the dimensionality of superconductivity, we analyze angular dependencies of the in-plane magnetoresistance $R(\Theta)$. As discussed in the Appendix, 3D and 2D cases can be unambiguously discriminated from the analysis of $R(\Theta)$ shapes close to the in-plane field orientation. In the 3D case there is a soft (parabolic) minimum with zero derivative, while in the 2D case there is a cusp with finite $dR/d\Theta$, as demonstrated by dashed (blue) and thin solid (red) lines in Fig. 2(e).

Figures 2(d) and 2(e) show measured $R(\Theta)$ for the same crystal at the applied field of 10 T and at several temperatures. $\Theta = 0°$ and $90°$ correspond to the field parallel and perpendicular to the ab plane, respectively. The 122 pnictides have a rather small anisotropy and even isotropic H_{c2} has been
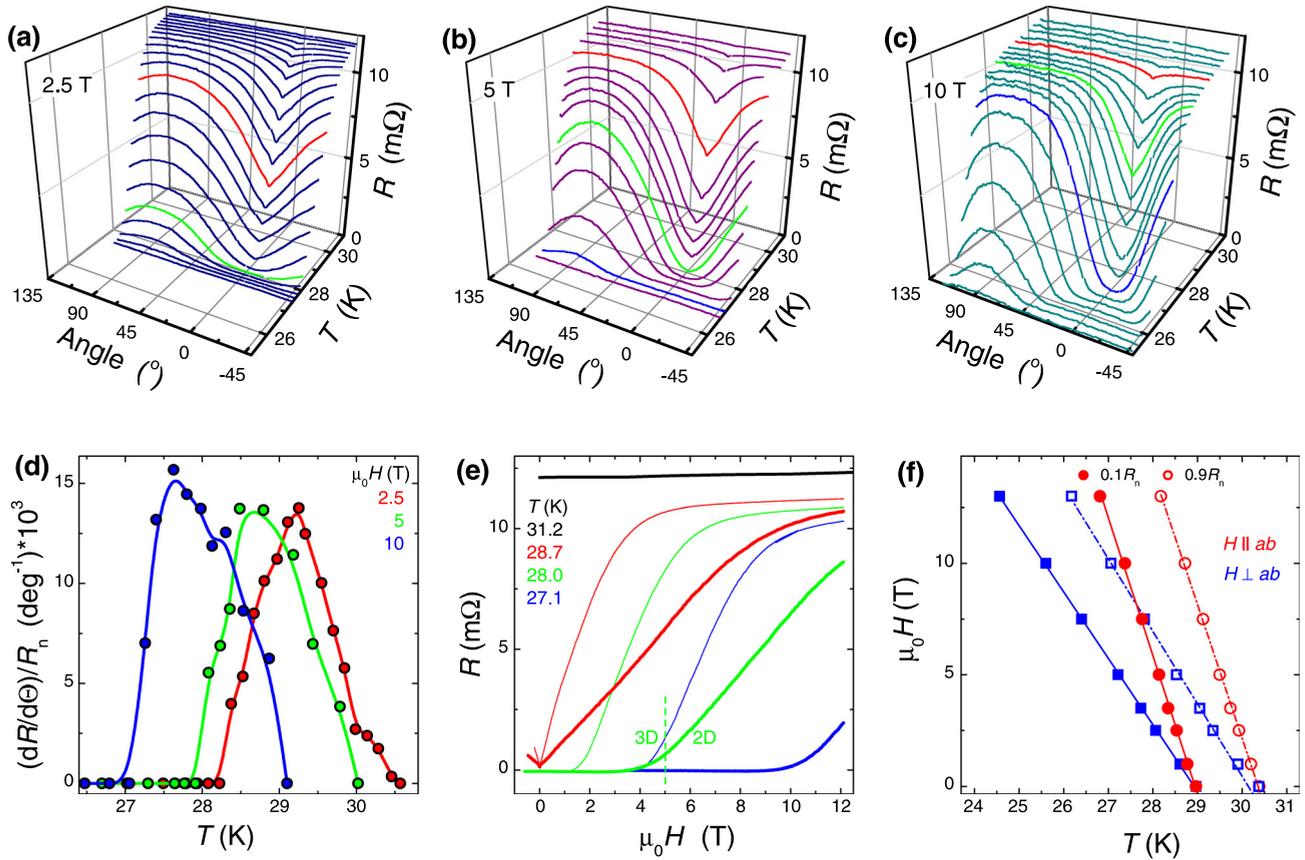
FIG. 3. Characteristics of a nearly optimally doped $Ba_{1-x}Na_xFe_2As_2$ single crystal $N.2$ with approximately three times larger thickness than the crystal $N.1$. (a)–(c) Angular dependence of in-plane resistance at fields (a) 2.5 T, (b) 5 T, and (c) 10 T. The 2D behavior in the resistive transition area appears at all fields. (d) Temperature dependencies of the cusp sharpness at 2.5, 5, and 10 T. (e) Field dependencies of resistance $R(H)$ at different temperatures for perpendicular (thin) and parallel (thick lines) fields at different T. For $T = 28$ K, a field-induced 3D-2D transition is indicated by the dashed line. (f) Temperature dependencies of field corresponding to 10% (solid symbols and lines) and 90% (open symbols, dashed-dotted lines) of the resistive transition.

reported [11], although the latter may not reflect the actual anisotropy in this case when H_{c2} is close to the paramagnetic limit [37]. From Fig. 2(c) it follows that the anisotropy $H_{\parallel}/H_{\perp}$ is ranging from $\gamma = 1.64$ for $R/R_n = 0.1$ to $\gamma = 2.06$ for $R/R_n = 0.9$. As discussed in the Introduction, this does not exceed the threshold value γ_{cr} for being considered as a layered superconductor. Consistently, bulk superconductivity in the studied crystal at low T and $H < H_{c2}$ has a weakly anisotropic 3D character. This is seen from the angular dependence of resistance at $T \sim 20$ K in Fig. 2(e) with a flat parabolic minimum at $\Theta = 0$.

However, at higher temperature and larger resistance a qualitative modification of $R(\Theta)$ curves occurs: they acquire a characteristic for the 2D superconductivity sharp cusp at $\Theta = 0$ [12,17,22,38]. With increasing temperature the cusp becomes sharper, but loses the amplitude and eventually disappears above $T > 28$ K. From comparison with the standard 2D dependence (for details see the Appendix) for a given amplitude of magnetoresistance [see the red line in Fig. 2(e)], it is seen that at higher T, close to the top of the resistive transition, the angular dependence becomes extremely sharp, much sharper than even the standard 2D dependence. As discussed in the Appendix, such an extreme 2D behavior can be expected when the field exceeds the

upper critical field $H > H_{c2}(\perp, T)$. This squeezes the range of angles for existence of bulk superconductivity to the vicinity of the in-plane orientation [37]. Furthermore, above H_{c2} bulk superconductivity is suppressed and only 2D surface superconductivity is persisting up to $H_{c3} \simeq 1.7 H_{c2}$ [22]. The latter indeed may lead to appearance of extraordinary sharp cusps, caused by nonlinearity of current-voltage characteristics [21]. The surface superconductivity always has the 2D character and can be observed even in isotropic superconductors [21,27,39].

Figure 2(f) shows temperature dependence of the absolute value of the angular derivative $dR/d\Theta(0)$. It clearly shows how a fairly abrupt 3D (small $dR/d\Theta$) to 2D (large $dR/d\Theta$) transition takes place at $T \simeq 21$ K. Contrary to the conventional 3D-2D crossover in layered superconductors, it occurs with *increasing* temperature.

Figure 3 represents similar data for a second Ba_{1-x} $Na_xFe_2As_2$ crystal $N.2$ from the same batch. The measured normal-state resistance of this sample is approximately three times smaller than for the crystal $N.1$ (Fig. 2). Since the contact configuration is exactly the same, we conclude that the $N.2$ crystal is approximately three times thicker than the $N.1$. It also has a sharper resistive transition with a higher midpoint $T_c \simeq 29.7$ K at $H = 0$. The difference in T_c for the two samples indicates that the doping state of the crystals

is somewhat affected by the processing (thin-film deposition and plasma etching), which is equivalent to soft annealing in vacuum during several hours. Thinner crystals are apparently affected stronger than thicker crystals, suggesting that the out-diffusion of dopants during annealing occurs predominantly in the c-axis direction. This is due to a flakelike geometry of our crystals with the thickness (just a few microns) much smaller than the lateral sizes (several hundreds of microns). Despite the difference in T_c, the general behavior of the two $Ba_{1-x}Na_xFe_2As_2$ crystals is similar.

Figures 3(a)–3(c) show angular dependencies of the in-plane resistance at different temperatures for applied fields of (a) 2.5 T, (b) 5 T, and (c) 10 T. It is seen that the 2D behavior appears with increasing T at all shown fields, qualitatively similar to that in Fig. 2(d). Quantitatively, however, the thinner crystal $N.1$ exhibits a more profound and sharper cusp in $R(\Theta)$ than the thicker $N.2$ crystal [cf. Figs. 2(d) and 3(c)]. This may indicate that the 2D behavior is originated from the surface of the crystal because the relative weight of the surface contribution decreases with increasing crystal thickness, following the surface-to-volume ratio.

Figure 3(d) represents the sharpness of the cusp in $R(\Theta)$ as a function of T for applied field of 2.5, 5, and 10 T. It is seen that the 2D behavior with a cusp occurs at all those fields, but the range of temperatures shifts to lower T with increasing field, following the corresponding shift of $T_c(H)$ [see Figs. 2(a) and 2(b)]. From this plot it also follows that at a given T the 2D behavior can be induced by the applied magnetic field. For example, at $T \simeq 28$ K the crystal is in the 3D state at 2.5 T, but turns into the 2D state above 5 T.

Figure 3(e) shows field dependencies of resistance $R(H)$ at different temperatures for perpendicular (thin) and parallel (thick lines) fields. For $T = 28$K (green), a field-induced 3D-2D transition is indicated by the dashed line. Interestingly, $R(H)$ is nonlinear in the 3D and linear in the 2D state. Linear-in-field $R(H)$ dependence is characteristic for pinning-free flux-flow regime [40]. Thus, the vortex pinning is essential in the 3D case and weak in the 2D state, as expected [18].

In Fig. 3(f) we show magnetic fields, corresponding to 10% and 90% of resistive transitions. The anisotropy is $\gamma \simeq 2$, consistent with that for the $N.1$ crystal [Fig. 2(c)]. Since the anisotropy is low, the $Ba_{1-x}Na_xFe_2As_2$ crystals should be considered as 3D superconductors. Interestingly, for both crystals the 2D behavior is observed when the measured resistance $R(H,T)$ exceeds $\sim 0.1R_n$. As shown in Ref. [21], this level is typical for $H \simeq H_{c2}$, at which the bulk superconductivity is destroyed.

B. 2D behavior in $Fe_{1+\delta}Te_{1-x}Se_x$ crystals

Figure 4(a) shows the in-plane resistance versus temperature at $H = 0$ for a $Fe_{1+\delta}Te_{1-x}Se_x$ crystal $N.3$, $x \simeq 0.28$. Unlike $Ba_{1-x}Na_xFe_2As_2$, it has a nonmetallic behavior with increasing resistance upon cooling down. Figures 4(b) and 4(c) show $R(T)$ transitions for the same sample, measured in different magnetic fields perpendicular [Fig. 4(b)] and parallel [Fig. 4(c)] to ab planes. It is seen that the superconducting transition has two steps a small one at $T_{c1} \simeq 7$ K and a larger at $T_{c2} \simeq 13$ K. Apparently, there is a significant spatial inhomogeneity with two dominant superconducting phases. Although

such a crystal does not seem to be an optimal object for studies, however, as we will argue below it emphasizes the robustness of 2D behavior even in a such an inhomogeneous sample.

Figure 4(d) represents field-temperature diagram in parallel (red) and perpendicular (blue) to ab-plane field orientations. Solid symbols/solid lines correspond to $\sim 10\%$ of the resistive transition, marked by the lower dashed lines in Figs. 4(b) and 4(c), which occurs also close to the top of the transition of the low-T_c phase. Open symbols/dashed-dotted lines correspond to 90% of the transition $R(T) \simeq 0.9R_n$, marked by top dashed lines in Figs. 4(b) and 4(c). Pluses/dashed lines correspond to the top of transitions $R(T) \simeq R_n$. The values of anisotropies $H_\parallel/H_\perp$ are $\gamma = 2.55$ for $R = 0.1R_n$, which corresponds primarily to the low-T_c phase, and $\gamma = 1.59$ for $R = 0.9R_n$, which corresponds primarily to the high-T_c phase. Those values are consistent with previous studies on $FeSe_{0.6}Te_{0.4}$ epitaxial thin films with a higher T_c [41].

Figure 4(e) shows temperature dependencies of $R(\Theta)$ at 10 T. Here again we see the qualitative modification of $R(\Theta)$ curves with *increasing* temperature. However, due to presence of two superconducting phases, we see two temperature-inverted 3D-2D transitions in $R(\Theta)$. The cusp originating from the low-T_c phase appears above ~ 2 K and is washed away above ~ 7 K, while the cusp from the high-T_c phase appears above 8 K and vanishes above ~ 14 K, as demonstrated in Fig. 4(f). Horizontal arrows in Fig. 4(d) mark the range of existence of 2D cusps in angular-dependent magnetoresistance, which are apparently connected with the range of resistive transitions of the two dominant superconducting phases [see Figs. 4(b) and 4(c)]. Despite an obviously strong inhomogeneity of this crystal, even in this case it is seen that the 2D behavior exists almost in the full range (from the bottom $R \sim 0$ to the top $R \sim R_n$) of the corresponding two resistive transitions.

IV. DISCUSSION

In Table I we summarize parameters of the studied crystals, such as estimated characteristic fields at $T = 0$, coherence lengths $\xi(T = 0)$, and corresponding anisotropies of $\xi(0)$. Here, $H_{\perp,\parallel}(0)$ represent results of the linear extrapolation to $T = 0$ of the measured linear experimental dependencies $H(T)$ from Figs. 2(c), 3(f), and 4(d). For comparison, we also show extrapolated values of the upper critical field, obtained using Werthamer-Helfand-Hohenberg (WHH) theory [42] for the clean case without spin-orbit effects: $H_{c2\parallel,\perp}(0) = 0.693T_c(dH_{\parallel,\perp}/dT)$. The values of ξ were obtained using relations $H_{c2\perp} = \phi_0/2\pi\xi_\parallel^2$ and $H_{c2\parallel} = \phi_0/2\pi\xi_\parallel\xi_\perp$. For both $Ba_{1-x}Na_xFe_2As_2$ crystals, $\mu_0H_{c2\perp}(0)$ is close to the paramagnetic field $B_p(0) = 1.84k_BT_c/\mu_B$, but $\mu_0H_{c2\parallel}(0)$ is twice larger than $B_p(0)$. For $FeSe_{1-x}Te_x$ crystal, both $\mu_0H_{c2\parallel,\perp}$ are larger than $B_p(0)$. Such an exercise demonstrates significance of spin-orbit coupling in both types of iron-based superconductors, consistent with data obtained in higher fields [11].

As follows from our data, both types of studied iron-based superconductors exhibit 2D behavior in magnetic field at elevated temperatures. We want to emphasize that the 2D behavior is unexpected for these compounds with a relatively low anisotropy $\gamma \sim 2$ (see Table I). Furthermore, the reported 3D-2D transition is temperature inverted with respect to

TABLE I. Estimated parameters of studied crystals. $dH_{\parallel,\perp}/dT$ and $H_{\parallel,\perp}(0)$ are slopes and linear extrapolations to $T = 0$, of field-temperature diagrams in Figs. 2(c), 3(f), and 4(d); T_c is the mean value of the critical temperature at zero magnetic field; $H_{c2\parallel,\perp}(0)$ is the upper critical field obtained from the WHH fit [42]; $\xi_{\parallel,\perp}$ are coherence lengths at $T = 0$, estimated from $H_{c2\parallel,\perp}(0)$; and γ is the anisotropy of $\xi(0)$.

N	Compound	Criteria	$\mu_0 dH_{\parallel}/dT$ (T/K)	$\mu_0 dH_{\perp}/dT$ (T/K)	$\mu_0 H_{\parallel}(0)$ (T)	$\mu_0 H_{\perp}(0)$ (T)	T_c (K)	$\mu_0 H_{c2\parallel}(0)$ (T)	$\mu_0 H_{c2\perp}(0)$ (T)	$\xi_{\parallel}$ (nm)	$\xi_{\perp}$ (nm)	γ $\xi_{\parallel}/\xi_{\perp}$
		$0.9R_n$	-4.87	-2.36	134.94	64.81	27.58	93.1	45.12	2.70	1.31	2.06
1	$Ba_{1-x}Na_xFe_2As_2$	$0.1R_n$	-3.69	-2.25	89.29	53.53	24.02	61.44	37.46	2.96	1.81	1.64
		$0.9R_n$	-5.99	-3.24	181.95	97.80	30.28	125.7	68.00	2.20	1.19	1.85
2	$Ba_{1-x}Na_xFe_2As_2$	$0.1R_n$	-6.20	-2.98	179.37	86.15	28.92	124.3	59.74	2.35	1.13	2.08
		$0.9R_n$	-7.02	-4.42	92.87	58.45	13.23	64.38	40.53	2.85	1.79	1.59
3	$Fe_{1+\delta}Te_{1-x}Se_x$	$0.1R_n$	-12.06	-4.73	79.94	29.52	6.44	53.83	21.11	3.95	1.55	2.55

the 3D-2D crossover in layered superconductors. Layered superconductors are in the 2D state at low T but turn into the 3D state with $T \rightarrow T_c$ due to a divergence of the coherence length [12–17]. In our case, the situation is opposite: at low T both superconductors are in the 3D state, but start to exhibit the 2D behavior at elevated T close to T_c. Consequently, the observed 2D behavior is not related to intrinsic layeredness of the studied compounds. Below, we discuss two possible

"extrinsic" origins of the 2D behavior: (i) laminated crystal structure, and (ii) surface superconductivity.

A. Artificial lamination

An artificial 2D behavior may occur if crystals have a laminated structure with thin flakes along ab planes having a higher T_c. Since the T_c depends on the doping state, this
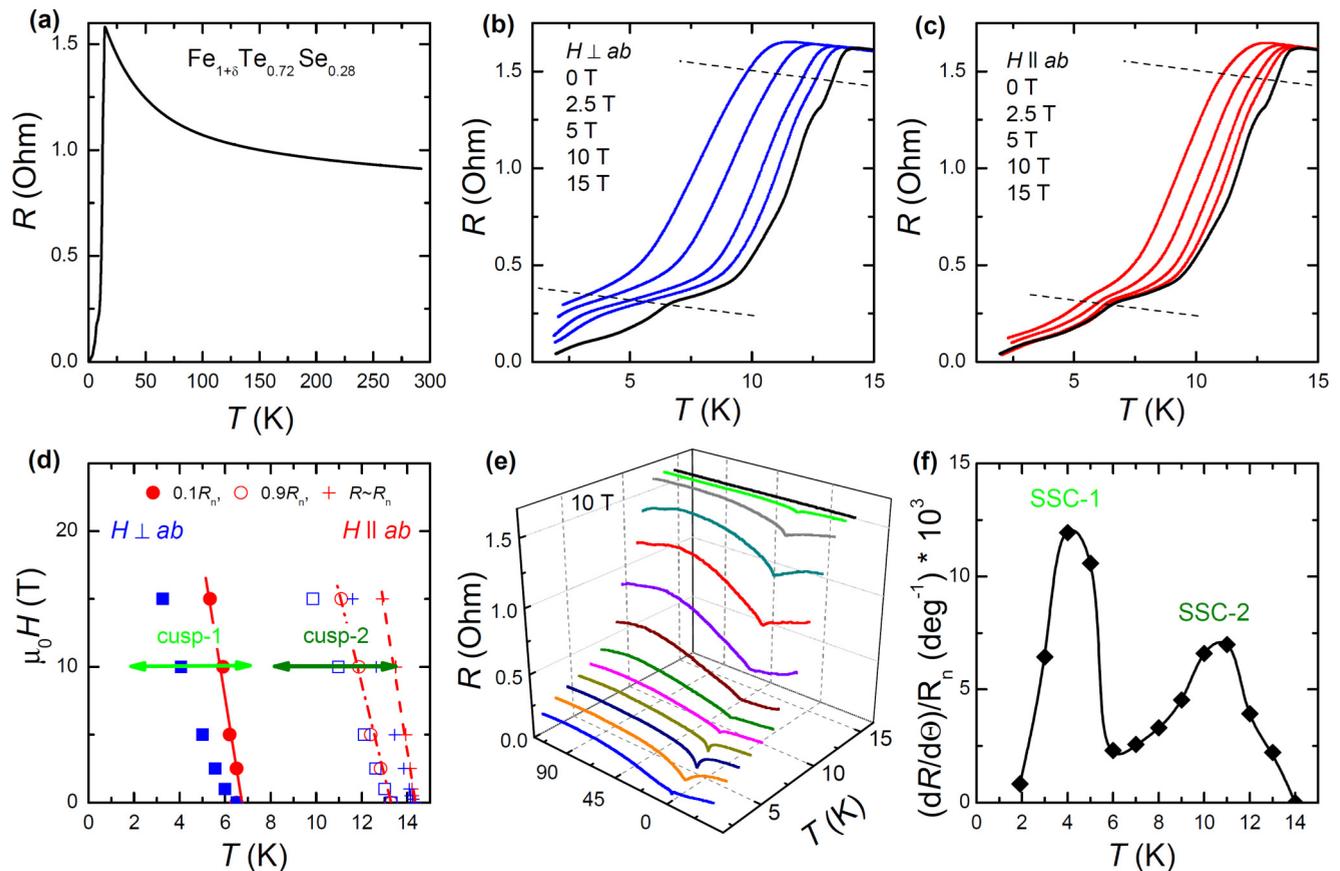
FIG. 4. (a) In-plane resistance versus temperature for a $Fe_{1+\delta}Te_{1-x}Se_x$ crystal in zero magnetic field. (b), (c) Resistive transitions in perpendicular (b) and parallel (c) fields of 0, 5, 10, and 15 T. (d) Temperature dependencies of the bottom $R \sim 0.1R_n$ (solid symbols and lines), $R \sim 0.9R_n$ (open symbols, dashed-dotted lines), and the top $R \sim R_n$ (plus symbols, dashed line) of the resistive transition in perpendicular (blue) and parallel (red) fields. Horizontal arrows indicate the range of temperatures at which 2D cusps occur in angular-dependent magnetoresistance at 10 T. (e) Angular dependence of resistance at 10 T and different temperatures. (f) The sharpness of the cusp as a function of temperature for the data from (e). Two distinct cusps are seen manifesting appearance of 2D superconductivity in each of the two dominant superconducting phases.

may be due to stratification of the dopant atoms, and not necessarily direct crystal defects. Certain spread of the doping concentration for both types of crystals is obvious from broadening of superconducting transitions in zero field. Such a stratification with two superconducting phases is apparent for $Fe_{1+\delta}Te_{1-x}Se_x$ crystals. However, the lamination may not explain all the observed features.

First of all, lamination does not lead to formation of a true multilayer in the c-axis direction because an artificial multilayer would still exhibit a regular 3D-2D crossover upon decreasing temperature. In this case, the diverging coherence length at $T \to T_c$ would ensure the 3D state of the multilayer at elevated temperatures. This is opposite to the reported behavior. Therefore, there could only be few flakes, separated by a relative large distance in the c-axis direction.

Second, for the phase-segregated $Fe_{1+\delta}Te_{1-x}Se_x$ crystals we observe two steps in the resistive transition with two corresponding 2D regions [see Fig. 4(f)]. This implies that the phases are in fact not flakelike but bulk. Indeed, a transition of few decoupled parallel to ab-plane flakes of the low-T_c phase into the normal state would not lead to a disruption of the supercurrent flow along the ab plane and, thus, would not be visible in experiment.

Third, true lamination should lead to the corresponding 2D behavior of the temperature dependence of the upper critical field $H_{c2}^{\parallel}(T) \propto \sqrt{1 - T/T_c}$, while the perpendicular field should have the same linear dependence as in the 3D case $H_{c2}^{\perp}(T) \propto 1 - T/T_c$. This has been reported both for artificial multilayers [12–17] and for layered cuprates [37]. Different temperature dependencies should lead to a large anisotropy of H_{c2} close to T_c, $H_{c2}^{\parallel}/H_{c2}^{\perp}(T) \propto 1/\sqrt{1 - T/T_c}$. However, all our samples for both studied compounds exhibit linear T dependencies $H_{c2}^{\parallel}(T) = \gamma H_{c2}^{\perp}(T) \propto 1 - T/T_c$ at both orientations with a relatively small $\gamma \sim 2$ [see Figs. 2(c), 3(f), and 4(d)]. Such a 3D temperature dependence of $H_{c2}^{\parallel}(T)$ does not support the assumption of artificial crystal lamination as the source of the observed 2D behavior.

B. Surface superconductivity

It is known that bulk 3D superconductors may exhibit 2D surface superconductivity in magnetic field parallel to the surface, larger than the bulk upper critical field, but lower than the third critical field $H_{c3} \simeq 1.7 H_{c2}$ [22]. SSC has been observed in a variety of superconductors, including conventional low-T_c [21,23–26], MgB_2 [27,28], and some pnictides [29]. In the latter case, a very large $H_{c3}/H_{c2} \simeq 4.4$ ratio has been reported, suggesting an unusual robustness of SSC. Since SSC occurs only in the surface layer with the thickness $\xi_\perp$, it exhibits a pure 2D behavior.

Surface superconductivity can explain the unusual temperature-inverted appearance of the 2D behavior. Indeed, it is expected that at a fixed H such a 3D-2D bulk-to-surface transition would occur with increasing temperature when H exceeds $H_{c2}(T)$ and bulk superconductivity is suppressed. A similar 3D-2D bulk-to-surface transition occurs at a fixed T upon increasing of magnetic field above $H_{c2}(T)$ [21]. Such a field-induced 3D-2D transition is demonstrated in Figs. 3(d) and 3(e).

The variation of the cusp with the crystal thickness is also consistent with the SSC scenario. Indeed, the thinner crystal $N.1$ exhibits a more profound and sharper cusp in $R(\Theta)$ than the thicker $N.2$ [cf. Figs. 2(d) and 3(c)]. This is consistent with the corresponding increment of the surface to volume ratio with decreasing crystal thickness, which makes 2D SSC contribution more profound in the thinner crystal.

For $Fe_{1+\delta}Te_{1-x}Se_x$ appearance of 2D surface superconductivity for each of the two phases indicates that those phases are spatially segregated with sharp interfaces in-between. The appearance of 2D SSC definitely proves phase segregation, suspected in those compounds [32,34].

C. Determination of H_{c2} using 3D-2D bulk-to-surface transition

From Figs. 2(a)–2(c), it is seen that the resistive transition is broadened: the difference in T between 90% and 10% of the transition for the $N.1$ crystal is about 4 K. In this case, it becomes difficult to determine H_{c2} because there is no clear criterion if $H_{c2}(T)$ corresponds to the beginning, the middle, or the end of the transition. However, the appearance of SSC unambiguously pinpoints $H_{c2}^{\parallel}(T) = H$, as indicated by the dashed line in Fig. 2(f). The horizontal arrow in Fig. 2(c) indicates the range of temperatures for which a 2D cusp in $R(\Theta)$ appears. It is seen that 2D behavior appears when the resistance reaches $\sim$10% of the normal resistance and persists up to the very top of the resistive transition. Thus, H_{c2} corresponds to the bottom of the resistive transition, $R \sim 0.1 R_n$, while the rest of the transition is strongly affected by surface superconductivity. This is consistent with a previous conclusion [21] that surface superconductivity is making a major contribution to broadening of the resistive transition in magnetic field. Importantly, the onset of surface superconductivity allows unambiguous determination of $T_c(H)$ or, equivalently $H_{c2}(T)$, which are most closely represented by solid lines in Fig. 2(c).

V. CONCLUSIONS

To conclude, we observed an unexpected 2D behavior in low anisotropic iron-based superconductors. Contrary to the conventional dimensional 3D-2D crossover in layered superconductors, it appears upon *increasing* of temperature. Based on the similar observation in isotropic Nb films [21], we argue that this type of temperature-inverted 3D-2D transition is caused by transition from 3D bulk to 2D surface superconductivity. Such a transition occurs with increasing T when the applied field becomes larger than the temperature-dependent upper critical field $H > H_{c2}(T_{2D})$. The 2D state persists up to a temperature at which the field exceeds the temperature-dependent third critical field $H > H_{c3}(T)$.

The data presented above demonstrate that surface superconductivity is a common phenomenon both for conventional low-T_c and unconventional high-T_c superconductors. Moreover, it is a very robust phenomenon and occurs not only in perfect single crystals. Our data indicate that SSC remains profound in a strongly inhomogeneous $Fe_{1+\delta}Te_{0.72}Se_{0.28}$ chalcogenide with two dominant superconducting phases. Furthermore, we observe that 2D surface superconductivity persists up to the very end of the resistive transition $R \simeq R_n$.

This implies that SSC is making a significant contribution to broadening of the superconducting transition in magnetic field, consistent with a previous report [21]. This may strongly affect [21] the standard analysis of superconducting fluctuations, which does not take into consideration persistence of nonfluctuating SSC (see, for example, [43]).

Finally, we point out that determination of the upper critical field for unconventional superconductors remains notoriously difficult and controversial [44]. The high T_c leads to an extended region of thermally activated flux flow. The complex physics of anisotropic pinning and melting of the vortex lattice [18] makes it hard, if at all possible, to confidently obtain H_{c2} from flux-flow characteristics at $T < T_c(H)$. The situation is further complicated by ill-defined normal state due to persistence the normal-state pseudogap, inhomogeneity of doping, strong superconducting fluctuations, and, as we show in this work also the surface superconductivity phenomenon. All of them lead to significant broadening of superconducting transitions so that it becomes hard to ascribe any specific point at the $R(T,H)$ curve to $H = H_{c2}$. As we have shown above, the reported bulk-to-surface superconductivity transition removes this ambiguity. Bulk superconductivity is suppressed at $H = H_{c2}$. Therefore, the appearance of a well-defined cusp in angular dependence of magnetoresistance can be used for unambiguous determination of the upper critical field. Therefore, we encourage other researchers to use this phenomenon for correct determination of H_{c2}.

APPENDIX A: ANGULAR DEPENDENCIES OF MAGNETORESISTANCE IN 3D AND 2D CASES

In this appendix, we intend to demonstrate that the cusp in $R(\Theta)$ is an unambiguous signature of the 2D behavior. Angular dependencies of critical fields for anisotropic 3D and 2D cases are given by the following equations (see, e.g., Ref. [38]):

$$\left(\frac{H_{c2}(\Theta)\sin\Theta}{H_{c2}^{\perp}}\right)^2 + \left(\frac{H_{c2}(\Theta)\cos\Theta}{H_{c2}^{\parallel}}\right)^2 = 1 \qquad \text{(A1)}$$

for the 3D case, and

$$\left|\frac{H_{c2}(\Theta)\sin\Theta}{H_{c2}^{\perp}}\right| + \left(\frac{H_{c2}(\Theta)\cos\Theta}{H_{c2}^{\parallel}}\right)^2 = 1 \qquad \text{(A2)}$$

for the 2D case.

In the simplest case, the flux-flow resistivity in magnetic field can be estimated from the Bardeen-Stephen expression [40]

$$R(\Theta) = R_n \frac{H}{H_{c2}(\Theta)}. \qquad \text{(A3)}$$

The corresponding examples of $R(\Theta)$ obtained from Eqs. (A1)–(A3) are shown by blue and red lines in Fig. 2(e). The main qualitative difference between them is that $R(\Theta = 0)$ has a flat (parabolic) minimum with $dR/d\Theta(\Theta = 0) = 0$ in the 3D case and a cusplike dip with finite $dR/d\Theta(\Theta = \pm 0) \neq 0$ in the 2D case, reflecting corresponding angular dependencies of critical fields from Eqs. (A1) and (A2), respectively.

We note that the agreement of experimental data with such curves is only qualitative. The main reason is that 3D/2D models yield angular dependencies of critical fields, not of the measured resistances. The straightforward connection between $H_{c2}(\Theta)$ and $R(\Theta)$ using Eq. (A3) is an oversimplification because it neglects pinning of vortices and assumes a linear field dependence of resistivity (A3), which is not always the case. Vortex pinning in the 3D case makes $R(H)$ nonlinear, as shown in Fig. 3(e) and in particular leads to dropping of $R(T)$ to zero below certain T [see Figs. 1(a) and 1(b)].

Due to oversimplifications of the models based on Eqs. (A1)–(A3), we do not expect quantitative fits, but only qualitative behavior a flat minimum in the 3D versus a sharp cusp in the 2D case. In the absence of the exact fit, one can ask how ambiguous is the interpretation of the observed cusp as evidence of the 2D behavior. In other words, could a similar cusp appear under some circumstances even in the 3D case? To understand this, we analyze more rigorously the shape of $R(\Theta)$ for 3D anisotropic superconductors, using a scaling approach by Blatter and co-workers [45]. According to them, in an anisotropic 3D case there is a universal scaling (see, e.g., Ref. [20])

$$R(\Theta) = F(\widetilde{H}), \quad \widetilde{H} = H\sqrt{\sin^2\Theta + \gamma^{-2}\cos^2\Theta}. \qquad \text{(A4)}$$

We remind that in our definition $\Theta = 0$ corresponds to in-plane (ab) and $90°$ to out-of-plane (c-axis) magnetic field. For the derivative we obtain

$$\frac{dR}{d\Theta} = \frac{\partial F}{\partial \widetilde{H}} H \frac{\sin\Theta\cos\Theta(1 - \gamma^{-2})}{\sqrt{\sin^2\Theta + \gamma^{-2}\cos^2\Theta}}. \qquad \text{(A5)}$$

In Fig. 5(a), we show corresponding variation of $dR/d\Theta$ with increasing the anisotropy from isotropic $\gamma = 1$ (zero line coincident with the horizontal axis) to strongly anisotropic $\gamma = 100$. Importantly, irrespective of γ, $dR/d\Theta(\Theta = 0) = 0$ due to $\sin\Theta$ term in the nominator of Eq. (A5).

From Eq. (A5) we obtain an asymptotic behavior close to the in-plane orientation

$$R(\Theta \sim 0) \simeq R(0)\left[1 + \frac{\Theta^2(\gamma - \gamma^{-1})}{2}\right]. \qquad \text{(A6)}$$

The corresponding parabolic angular dependencies are shown in Fig. 5(b). It is seen that although angular dependencies become stronger with increasing γ, however, even for a very large $\gamma = 100$ there is an unmistakable flat minimum $R(\Theta = 0)$ within several degrees from the in-plane orientation. It is
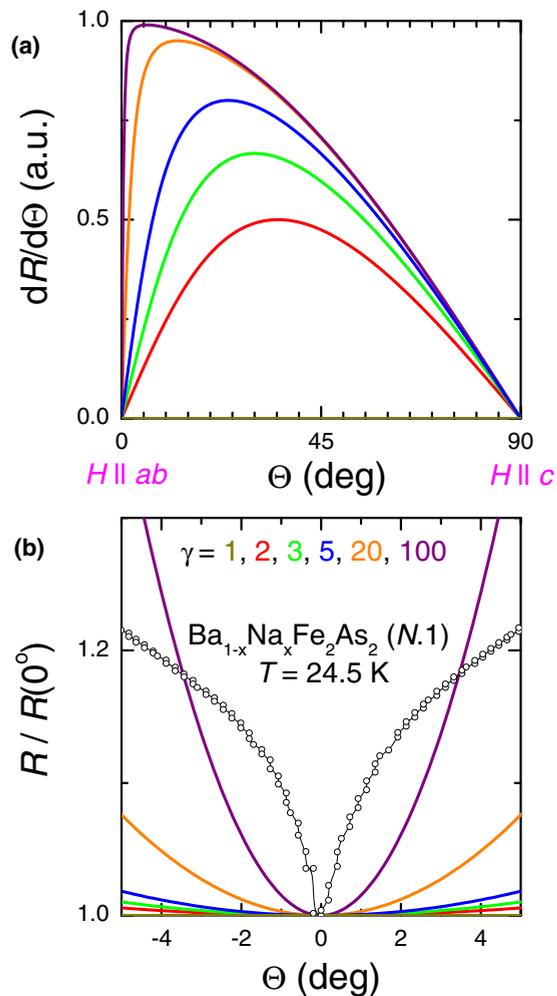
FIG. 5. Simulated angular dependencies for the 3D scaling model from Ref. [45] for different values of the anisotropy parameter γ from 1 to 100. (a) Angular derivatives. (b) Asymptotic behavior of $R(\Theta)$ near in-plane field. Note that $R(\Theta \to 0)$ has a parabolic behavior with a flat minimum and zero derivative $dR/d\Theta$, irrespective of γ. This is qualitatively different from the cusp behavior in the 2D case. Black symbols represent experimental cusplike behavior for the N.1 crystal, which quite apparently can not be fitted by the 3D model.

much coarser than the angular resolution of our measurement. For comparison, we show by black open circles experimental data for the N.1 crystal from Fig. 2(e) at $T = 25.4$ K. Quite apparently, it can not be fitted by the 3D model.

APPENDIX B: SCALING ANALYSIS OF THE 3D CASE

Another way to distinguish 3D from 2D behavior is to analyze how well the 3D scaling (A4) is satisfied.
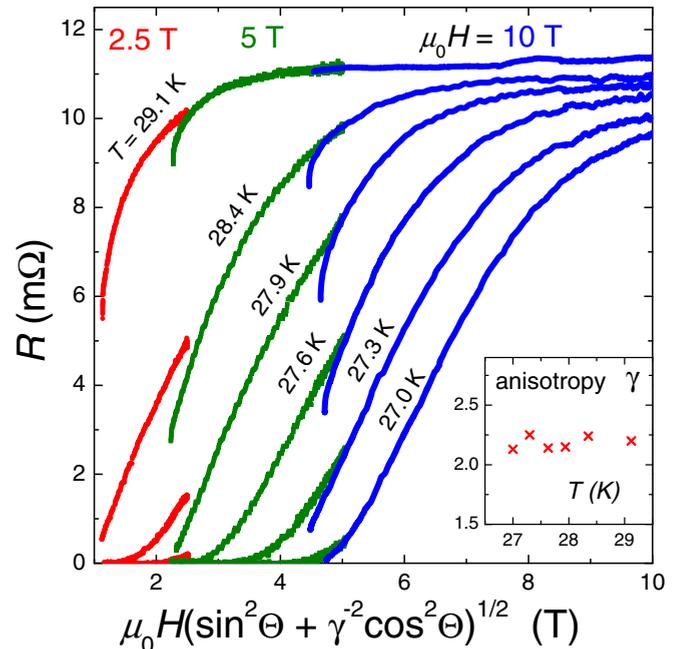
FIG. 6. Analysis of 3D scaling of angular-dependent magnetoresistance according to Eq. (A4) at different temperatures and at fields 2.5 T (red), 5 T (olive), and 10 T (blue curves) for the N.2 BNFA crystal. It is seen that the 3D scaling fails in the vicinity of parallel to the planes orientation of the field (the left ends of the curves), at which there is a rapid falloff from the smooth 3D behavior. The inset shows the anisotropy γ, which is the only free parameter in the scaling.

In Fig. 6, we show the corresponding scaling R versus $H(\sin^2 \Theta + \gamma^{-2} \cos^2 \Theta)^{1/2}$ for the N.2 BNFA crystal at different temperatures and fields. The only free parameter for such scaling is the anisotropy γ. It is shown in the inset in Fig. 6. It is seen that $\gamma \simeq 2.2$ is constant, as expected in the Ginzburg-Landau limit close to T_c, and has a value consistent with earlier estimations made in a similar way for a similar K-doped pnictide [20] and with our estimations above, see Table I. The 3D behavior in this scale is quasilinear [20] in the intermediate angle range $0 \ll \Theta \ll 90°$, as seen for the curve at the lowest $T = 27$ K, where the soft 3D angular dependence of magnetoresistance is observed [see the blue line in Fig. 3(c)]. At higher T, when the 2D cusp appears in $R(\Theta)$ at $\Theta = 0$, a clear falloff from the quasilinear 3D behavior occurs at the left edges of the curves, corresponding to the cusp region $\Theta = 0$. This is particularly well seen for $T = 27.6, 27.9$, and 28.4 K at $\mu_0 H = 10$ T and for $T = 29.1$ K at $\mu_0 H = 5$ T. This discrepancy confirms that the observed cusp in the angular dependencies of magnetoresistance can not be confused with 3D characteristics and, therefore, indeed is an unambiguous indication for appearance of the 2D behavior.

[1] V. L. Ginzburg, The problem of high-temperature superconductivity. II, Sov. Phys. Usp. **13**, 335 (1970).

[2] R. Kleiner and P. Müller, Intrinsic Josephson effects in high-Tc superconductors, Phys. Rev. B **49**, 1327 (1994).

[3] M. Nagao, S. Urayama, S. M. Kim, H. B. Wang, K. S. Yun, Y. Takano, T. Hatano, I. Iguchi, T. Yamashita, M. Tachiki *et al.*, Periodic oscillations of Josephson-vortex flow resistance in oxygen-deficient YBa$_2$Cu$_3$O$_x$, Phys. Rev. B **74**, 054502 (2006).

[4] S. O. Katterwe and V. M. Krasnov, Stabilization of the in-phase fluxon state by geometrical confinement in small $Bi_2Sr_2CaCu_2O_{8+x}$ mesa structures, Phys. Rev. B **80**, 020502(R) (2009).

[5] C. Liu, T. Kondo, N. Ni, A. D. Palczewski, A. Bostwick, G. D. Samolyuk, R. Khasanov, M. Shi, E. Rotenberg, S. L. Budko *et al.*, Three- to Two-Dimensional Transition of the Electronic Structure in $CaFe_2As_2$: A Parent Compound for an Iron Arsenic High-Temperature Superconductor, Phys. Rev. Lett. **102**, 167004 (2009).

[6] Yu. V. Pustovit and A. A. Kordyuk, Metamorphoses of electronic structure of FeSe-based superconductors (Review article), Low Temp. Phys. **42**, 995 (2016).

[7] P. J. W. Moll, L. Balicas, V. Geshkenbein, G. Blatter, J. Karpinski, N. D. Zhigadlo, and B. Batlogg, Transition from slow Abrikosov to fast moving Josephson vortices in iron pnictide superconductors, Nat. Mater. **12**, 134 (2013).

[8] P. J. W. Moll, X. Zhu, P. Cheng, H. H. Wen, and B. Batlogg, Intrinsic Josephson junctions in the iron-based multiband superconductor $(V_2Sr_4O_6)Fe_2As_2$, Nat. Phys. **10**, 644 (2014).

[9] J. Murphy, M. A. Tanatar, D. Graf, J. S. Brooks, S. L. Budko, P. C. Canfield, V. G. Kogan, and R. Prozorov, Angular-dependent upper critical field of overdoped $Ba(Fe_{1-x}Ni_x)_2As_2$, Phys. Rev. B **87**, 094505 (2013).

[10] Y. Liu, M. A. Tanatar, W. E. Straszheim, B. Jensen, K. W. Dennis, R. W. McCallum, V. G. Kogan, R. Prozorov, and T. A. Lograsso, Comprehensive scenario for single-crystal growth and doping dependence of resistivity and anisotropic upper critical fields in $(Ba_{1-x}K_x)Fe_2As_2$ ($0.22 \leqslant x \leqslant 1$), Phys. Rev. B **89**, 134504 (2014).

[11] H. Q. Yuan, J. Singleton, F. F. Balakirev, S. A. Baily, G. F. Chen, J. L. Luo, and N. L. Wan, Nearly isotropic superconductivity in $(Ba, K)Fe_2As_2$, Nature (London) **457**, 565 (2009).

[12] I. Banerjee and I. K. Schuller, Transition Temperatures and Critical Fields of Nb/Cu Superlattices, J. Low Temp. Phys. **54**, 501 (1984).

[13] R. A. Klemm, A. Luther, and M. R. Beasley, The upper critical field in layered superconductors, Phys. Rev. B **12**, 877 (1975).

[14] S. Takahashi and M. Tachiki, Theory of the upper critical field of superconducting superlattices, Phys. Rev. B **33**, 4620 (1986).

[15] V. M. Krasnov, N. F. Pedersen, V. A. Oboznov, and V. V. Ryazanov, Josephson properties of Nb/Cu multilayers, Phys. Rev. B **49**, 12969 (1994).

[16] V. M. Krasnov, A. E. Kovalev, V. A. Oboznov, and N. F. Pedersen, Magnetic field decoupling and 3D-2D crossover in Nb/Cu multilayers, Phys. Rev. B **54**, 15448 (1996).

[17] C. Attanasio, C. Coccorese, L. V. Mercaldo, M. Salvato, L. Maritato, A. N. Lykov, S. L. Prischepa, and C. M. Falco, Angular dependence of the upper critical field in Nb/CuMn multilayers, Phys. Rev. B **57**, 6056 (1998).

[18] L. I. Glazman and A. E. Koshelev, Thermal fluctuations and phase transitions in the vortex state of a layered superconductor, Phys. Rev. B **43**, 2835 (1991).

[19] F. F. Yuan, Y. Sun, W. Zhou, X. Zhou, Q. P. Ding, K. Iida, R. Huhne, L. Schultz, T. Tamegai, and Z. X. Shi, Anisotropy of iron-platinum-arsenide $Ca10(PtnAs8)(Fe2-xPtxAs2)5$ single crystals, Appl. Phys. Lett. **107**, 012602 (2015).

[20] Z. S. Wang, H. Q. Luo, C. Ren, and H. H. Wen, Upper critical field, anisotropy, and superconducting properties of $Ba_{1-x}K_xFe_2As_2$ single crystals, Phys. Rev. B **78**, 140501(R) (2008).

[21] A. Zeinali, T. Golod, and V. M. Krasnov, Surface superconductivity as the primary cause of broadening of superconducting transition in Nb-films, Phys. Rev. B **94**, 214506 (2016).

[22] D. Saint-James, G. Sarma, and E. J. Thomas, *Type-II Superconductivity* (Pergamon, Oxford, NY, 1969).

[23] S. Casalbuoni, E. A. Knabbe, J. Kötzler, L. Lilje, L. von Sawilski, P. Schmüser, and B. Steffen, Surface superconductivity in niobium for superconducting RF cavities, Nucl. Instrum. Methods Phys. Res., Sect. A **538**, 45 (2005).

[24] R. V. Bellau, Influence of surface condition on the critical currents above Hc2 in a superconducting Tantalum-Niobium alloy, Phys. Lett. **21**, 13 (1966).

[25] S. R. Park, S. M. Choi, D. C. Dender, J. W. Lynn, and X. S. Ling, Fate of the Peak Effect in a Type-II Superconductor: Multicriticality in the Bragg-Glass Transition, Phys. Rev. Lett. **91**, 167003 (2003).

[26] P. Das, C. V. Tomy, S. S. Banerjee, H. Takeya, S. Ramakrishnan, and A. K. Grover, Surface superconductivity, positive field cooled magnetization, and peak-effect phenomenon observed in a spherical single crystal of niobium, Phys. Rev. B **78**, 214504 (2008).

[27] A. Rydh, U. Welp, J. M. Hiller, A. E. Koshelev, W. K. Kwok, G. W. Crabtree, K. H. P. Kim, K. H. Kim, C. U. Jung, H.-S. Lee *et al.*, Surface contribution to the superconducting properties of MgB_2 single crystals, Phys. Rev. B **68**, 172502 (2003).

[28] H.-S. Lee, D.-J. Jang, B. Kang, H.-G. Lee, I. J. Lee, Y. Jo, M.-H. Jung, M.-H. Cho, and S.-I. Lee, Relationship between surface superconductivity, bulk superconductivity and the peak effect in MgB_2 single crystals, New J. Phys. **10**, 063003 (2008).

[29] M. I. Tsindlekht, I. Felner, M. Zhang, A. F. Wang, and X. H. Chen, Superconducting critical fields of single-crystalline $K_{0.73}Fe_{1.68}Se_2$, Phys. Rev. B **84**, 052503 (2011).

[30] S. Aswartham, M. Abdel-Hafiez, D. Bombor, M. Kumar, A. U. B. Wolter, C. Hess, D. V. Evtushinsky, V. B. Zabolotnyy, A. A. Kordyuk, T. K. Kim *et al.*, Hole doping in $BaFe_2As_2$: The case of $Ba_{1-x}Na_xFe_2As_2$ single crystals, Phys. Rev. B **85**, 224520 (2012).

[31] A. A. Kordyuk, Iron-based superconductors: Magnetism, superconductivity, and electronic structure (Review Article), Low Temp. Phys. **38**, 888 (2012).

[32] Y. A. Ovchenkov, D. A. Chareev, E. S. Kozlyakova, O. S. Volkova, and A. N. Vasiliev, Coexistence of superconductivity and magnetism in $Fe_{1+d}Te_{1-x}Se_x$ ($x = 0.1, 0.2, 0.28, 0.4$ and 0.45), Phys. C (Amsterdam) **489**, 32 (2013).

[33] D. A. Chareev, E. Osadchii, T. Kuzmicheva, Y. Y. Lin, S. Kuzmichev, O. Volkova, and A. Vasiliev, Single crystal growth and characterization of tetragonal $FeSe_{1-x}$ superconductors, CrystEngComm **15**, 1989 (2013).

[34] K. Prokeš, M. Schulze, S. Hartwig, N. Schäfer, S. Landsgesell, C. G. F. Blum, D. Abou-Ras, M. Y. Hacisalihoglu, E. Ressouche, B. Ouladdiaf, B. Büchner, and S. Wurmehl, Structural inhomogeneities in $FeTe_{0.6}Se_{0.4}$: Relation to superconductivity, J. Cryst. Growth **432**, 95 (2015).

[35] V. M. Krasnov, T. Bauch, and P. Delsing, Probing the intrinsic Josephson coupling potential in $Bi_2Sr_2CaCu_2O_{8+\delta}$ superconductors by thermal activation, Phys. Rev. B **72**, 012512 (2005).

[36] V. M. Krasnov, H. Motzkau, T. Golod, A. Rydh, S. O. Katterwe, and A. B. Kulakov, Comparative analysis of tunneling magnetoresistance in low-Tc Nb/Al-AlOx/Nb and high-T_c $Bi_{2-y}Pb_ySr_2CaCu_2O_{8+d}$ intrinsic Josephson junction, Phys. Rev. B **84**, 054516 (2011).

[37] S. O. Katterwe, Th. Jacobs, A. Maljuk, and V. M. Krasnov, Low anisotropy of the upper critical field in a strongly anisotropic layered cuprate $Bi_{2.15}Sr_{1.9}CuO_{6+\delta}$: Evidence for a paramagnetically limited superconductivity, Phys. Rev. B **89**, 214516 (2014).

[38] M. J. Naughton, R. C. Yu, P. K. Davies, J. E. Fischer, R. V. Chamberlin, Z. Z. Wang, T. W. Jing, N. P. Ong, and P. M. Chaikin, Orientational anisotropy of the upper critical field in single-crystal $YBa_2Cu_3O_7$ and $Bi_{2.2}CaSr_{1.9}Cu_2O_{8+x}$, Phys. Rev. B **38**, 9280 (1988).

[39] J. P. Burger, G. Deutscher, E. Guyon, and A. Martinet, Behavior of First- and Second-Kind Superconducting Films Near Their Critical Fields, Phys. Rev. **137**, A853 (1965).

[40] J. Bardeen and M. J. Stephen, Theory of the Motion of Vortices in Superconductors, Phys. Rev. **140**, A1197 (1965).

[41] D. Ahmad, W. J. Choi, Y. I. Seo, S. Seo, S. Lee, and Y. S. Kwon, Thermally activated flux flow in superconducting epitaxial $FeSe_{0.6}Te_{0.4}$ thin film, Res. Phys. **7**, 16 (2017).

[42] N. R. Werthamer, K. Helfand, and P. C. Hohenberg, Temperature and Purity Dependence of the Superconducting Critical Field, H_{c2}. III. Electron Spin and Spin-Orbit Effects, Phys. Rev. **147**, 295 (1966).

[43] M. Abdel-Hafiez, X.-M. Zhao, A. A. Kordyuk, Y.-W. Fang, B. Pan, Z. He, C.-G. Duan, J. Zhao, and X.-J. Chen, Enhancement of superconductivity under pressure and the magnetic phase diagram of tantalum disulfide single crystals, Sci. Rep. **6**, 31824 (2016).

[44] J. Chang, N. Doiron-Leyraud, O. Cyr-Choiniere, G. Grissonnanche, F. Laliberte, E. Hassinger, J-Ph. Reid, R. Daou, S. Pyon, T. Takayama *et al.*, Decrease of upper critical field with underdoping in cuprate superconductors, Nat. Phys. **8**, 751 (2012).

[45] G. Blatter, V. B. Geshkenbein, and A. I. Larkin, From Isotropic to Anisotropic Superconductors: A Scaling Approach, Phys. Rev. Lett. **68**, 875 (1992).